NASA Technical Paper 1367

An Analytical Technique for Predicting the Characteristics of a Flexible Wing Equipped With an Active Flutter-Suppression System and Comparison With Wind-Tunnel Data

Irving Abel

FEBRUARY 1979

NASA Technical Paper 1367

An Analytical Technique for Predicting the Characteristics of a Flexible Wing Equipped With an Active Flutter-Suppression System and Comparison With Wind-Tunnel Data

Irving Abel
Langley Research Center
Hampton, Virginia

NASA
National Aeronautics
and Space Administration

**Scientific and Technical
Information Office**

1979

SUMMARY

An analytical technique for predicting the performance of an active flutter-suppression system is presented. This technique is based on the use of an interpolating function to approximate the unsteady aerodynamics. The resulting equations are formulated in terms of linear, ordinary differential equations with constant coefficients. This technique is then applied to an aeroelastic model wing equipped with an active flutter-suppression system. Comparisons between wind-tunnel data and analysis are presented for the wing both with and without active flutter suppression. Results indicate that the wing flutter characteristics without flutter suppression can be predicted quite well but that a more adequate model of wind-tunnel turbulence is required when the active flutter-suppression system is used.

INTRODUCTION

A difficulty in analyzing active flutter-suppression systems lies in the modeling of the unsteady aerodynamic forces. These aerodynamic forces are normally computed only for simple harmonic motion at discrete values of reduced frequency. The use of harmonic motion for flutter analysis is adequate since the problem is one of finding the neutral stability boundary for which the motion continues with constant amplitude. The problem facing the analyst is one of modeling the unsteady aerodynamics for arbitrary motion.

In lieu of developing a completely new aerodynamic theory, there has been considerable interest in using the results of oscillatory unsteady aerodynamics to generate approximate solutions for arbitrary motion (refs. 1 to 4). This paper presents a method for analyzing active flutter-suppression systems. The method is based on a technique for approximating the unsteady aerodynamics in the time plane through an interpolating function in the frequency plane. By using the aerodynamic approximating function, the equations of motion are formulated in terms of linear, ordinary differential equations with constant coefficients. Active control functions are added to the equations in a straightforward and convenient manner. The resulting equations are reduced to a series of first-order differential equations which are solved to construct a root locus of the modes as a function of dynamic pressure. Also included is a method for calculating the response of the control system to turbulence.

The analytical method is then applied to an aeroelastic model equipped with an active flutter-suppression system. Comparisons between wind-tunnel data and analysis are presented for the wing flutter characteristics both with and without active flutter suppression. Also presented is a comparison of wind-tunnel data and analysis for the response of the active flutter-suppression system to tunnel turbulence.

SYMBOLS

$A_i(s)$	polynomial in s (see eqs. (B3))
a	speed of sound
b	reference semichord used in aerodynamic theory
c	streamwise local chord
D(s)	denominator polynomial in s of transfer function
D_m	feedback filter parameter
E	error function
$H(\omega)$	control surface frequency response function
j	$= \sqrt{-1}$
k	reduced frequency, $\omega b/V$
L	characteristic length in Von Kármán gust spectrum
L_s	wing span
l	Laplace transform operator
M	Mach number
M_i	generalized mass in ith vibration mode
m(x,y)	mass distribution
N(s)	numerator polynomial in s of transfer function
n	number of flexible modes
$\Delta p(x,y,t)$	pressure distribution
Q_i	generalized aerodynamic force in ith mode
Q_{ij}	generalized aerodynamic force in ith structural mode due to pressure distribution in jth mode
q	dynamic pressure, $\frac{1}{2}\rho V^2$
q_i	generalized displacement in ith mode
r	number of control surfaces

S	integration surface
s	$= j\omega$
t	time
V	free-stream velocity
w_g	gust velocity
x,y	streamwise and spanwise coordinates, respectively
$z(x,y)$	vertical deflection
β_i	aerodynamic lag
δ_a	control-surface deflection
δ_c, δ_c'	control-surface command and compensation, respectively
ζ	viscous damping coefficient
ρ	fluid density
σ_{w_g}	rms gust velocity
$\phi_I(\omega)$	Von Kármán gust spectrum
$\phi_i(x,y)$	normalized modal deflection in ith mode
ω	circular frequency
$\omega_{n,i}$	circular frequency of ith natural mode

Matrices:

$[A]$	matrix representing first-order equations of motion, system off
$[A_c]$	matrix representing first-order equations of motion, system on
$[A_i]$	real aerodynamic matrix coefficients
$[A_{i,\delta}]$	real aerodynamic matrix coefficients for control surfaces
$\{A_{i,g}\}$	real aerodynamic matrix coefficients for gust forces
$[\bar{A}]$. . .$[\bar{G}]$	see equations (B3)
$\{\hat{F}_G\}$	approximate aerodynamic gust vector
$[F_i]$	real coefficients of equations of motions

$[K]$ generalized stiffness matrix

$[M]$ generalized mass matrix

$[N]$ numerator polynomial in s of transfer function matrix

$[Q]$ matrix representing generalized aerodynamic forces

$[\hat{Q}]$ matrix representing approximate aerodynamic forces in the Laplace plane

$\{q\},\{\bar{q}\}$ complex response vectors

$[T]$ transfer function matrix

$\{X\}$ response vector of first-order equations of motion

$[\phi_t]$ matrix of modal deflection at sensor location

Subscripts:

c control

I imaginary part of complex value

max maximum

R real part of complex value

rms root-mean-square value

t sensor location

Dots over symbols denote derivatives with respect to time.

DESCRIPTION OF TECHNIQUE

Three-dimensional unsteady aerodynamics are normally computed, at a given Mach number, for simple harmonic motion at specific values of reduced frequency k. The control law for an active flutter-suppression system is usually given as a transfer function which relates control-surface motion to wing response. It is normally expressed as a ratio of polynomials in the transform variable s. The problem associated with the analysis of an active flutter-suppression system is developing a set of equations where the form of the unsteady aerodynamics and the control law are compatible. The approach taken in this report is to permit the variation of the aerodynamic forces with frequency to be approximated by a rational polynomial in the variable s. This technique is similar to that described in references 3 and 4.

The generalized aerodynamic forces are approximated in the s-plane through an interpolating function of the form

$$[\hat{Q}] = [A_0] + [A_1]\left(\frac{b}{V}\right)s + [A_2]\left(\frac{b}{V}\right)^2 s^2 + \sum_{m=3}^{6} \frac{[A_m]s}{\left(s + \frac{V}{b}\beta_{m-2}\right)} \qquad (1)$$

where $s = j\omega$ and $\beta_{m-2} = \omega_{m-2}b/V$. As described in reference 3, the form of equation (1) permits an approximation of the time delays inherent in unsteady aerodynamics subject to the following requirements: complex conjugate symmetry, denominator roots in the left-hand plane, and a good approximation of the complex aerodynamic terms at $s = j\omega$. The approximating coefficients (A_0, A_1, . . ., A_6) in equation (1) are evaluated by a least-squares curve fit (described in appendix A) through the values of complex aerodynamic terms at discrete values of reduced frequency. Figure 1 illustrates a typical fit through the values of complex aerodynamic coefficients. The solid curve represents the approximating function.

Wing Without Flutter-Suppression System

The equations of motion are formulated through a modal approach using Lagrange's equations of motion. In the modal approach, the elastic deformation at any point on the wing is described by a linear combination of orthogonal modes,

$$z(x,y,t) = \sum_{i=1}^{n} q_i(t)\ \phi_i(x,y)$$

where $\phi_i(x,y)$ are the undamped natural modes of the system and n is the number of modes used. Assuming a viscous form for structural damping, the equations of motion become

$$M_i\ \ddot{q}_i(t) + 2\zeta_i M_i \omega_{n,i}\ \dot{q}_i(t) + \omega_{n,i}^2 M_i\ q_i(t) = -\frac{1}{2}\rho V^2\ Q_i(t)$$

$$(i = 1, 2, \ldots, n) \qquad (2)$$

where

$$M_i = \iint_S m(x,y)\ \phi_i^2(x,y)\ dx\ dy$$

is the generalized mass and

$$Q_i(t) = \iint_S \frac{\Delta p(x,y,t)}{q}\ \phi_i(x,y)\ dx\ dy$$

is the generalized aerodynamic force. The total pressure distribution $\Delta p(x,y,t)$ can be expressed as the sum of the contributions due to each flexible mode. Therefore,

$$\Delta p(x,y,t) = \sum_{j=1}^{n} \Delta p_j(x,y)\ q_j(t)$$

where $\Delta p_j(x,y)$ is the lifting pressure at point (x,y) due to wing motion in the jth flexible mode. Substituting this expression for $\Delta p(x,y,t)$ into equation (2) results in

$$M_i \ddot{q}_i(t) + 2\zeta_i M_i \omega_{n,i} \dot{q}_i(t) + \omega_{n,i}^2 M_i\ q_i(t)$$

$$= -\frac{1}{2}\rho V^2 \sum_{j=1}^{n} \left[q_j(t) \iint_S \frac{\Delta p_j(x,y)}{q} \phi_i(x,y)\ dx\ dy \right] \tag{3}$$

where $i = 1, 2, \ldots, n$. By taking the Laplace transform of equation (3), the equations of motion can be written as

$$\left([M]s^2 + [2\zeta M\omega_n]s + \frac{1}{2}\rho V^2 \mathcal{L}([Q]) + [K] \right) \{q\} = 0 \tag{4}$$

where $\mathcal{L}$ is the Laplace transform operator, and

$$Q_{ij} = \iint_S \frac{\Delta p_j(x,y)}{q} \phi_i(x,y)\ dx\ dy$$

$$k_{ij} = \begin{cases} \omega_{n,i}^2 M_i & (i = j) \\ 0 & (i \neq j) \end{cases}$$

By substituting equation (1) into equation (4) and following the procedures outlined in appendix B, the equations of motion are reduced to a series of 6n first-order equations of the form

$$s\{X\} = [A]\{X\} \tag{5}$$

The eigenvalues of [A] are the roots of the characteristic flutter equations.

Wing With Flutter-Suppression System

The equations of motion are formulated in the same manner as described for the case with no control. For the wing equipped with an active flutter-suppression system, the equation which corresponds to equation (4) is

$$\left(\left[M \mid M_c\right] s^2 + \left[2\zeta M\omega_n \mid 0\right] s + \frac{1}{2}\rho V^2 l\left(\left[Q \mid Q_c\right]\right) + \left[K \mid K_c\right]\right)\left\{\frac{q}{---}\right\} = 0 \tag{6}$$

where

$[M_c]$ control-surface inertial coupling

$[K_c]$ control-surface stiffness coupling

$$[Q_c] = \iint_S \frac{\Delta p, q_c(x,y)}{q}\, \phi_i(x,y)\, dx\, dy$$

For a single control surface and a single sensor (accelerometer) the control-law transfer function can be assumed to be of the form

$$\frac{l(\delta_a)}{l(\ddot{z}_t)} = \frac{N(s)}{D(s)} \tag{7}$$

where

$$l(\ddot{z}_t) = s^2 \lfloor \phi_t \rfloor \{q\}$$

and

$$\delta_a = q_c$$

Therefore, equation (7) can be written as

$$q_c = \frac{s^2 N(s) \lfloor \phi_t \rfloor}{D(s)} \{q\} \tag{8}$$

where

$N(s)$ numerator polynomial in s

$D(s)$ denominator polynomial in s

and $\lfloor \phi_t \rfloor$ is a row matrix of modal deflections at the sensor location. Substituting equations (8) and (1) into equation (6) and following the procedures

outlined in appendix B, the equations of motion are written as a series of mn first-order equations of the form

$$s\{x\} = [A_c]\{x\} \tag{9}$$

where

m 6 + highest order term in D(s)

n number of modes

The eigenvalues of $[A_c]$ are the roots of the characteristic equation for the wing equipped with an active flutter-suppression system.

APPLICATION OF TECHNIQUE

To evaluate the adequacy of the analytical method in predicting the performance of an active flutter-suppression system, stability calculations were made for an aeroelastic wind-tunnel model equipped with an active flutter-suppression system. Tests were performed in the Langley transonic dynamics tunnel. A photograph of the model mounted in the wind tunnel is shown in figure 2. Model geometry is given in figure 3.

As input to the analysis it is necessary to determine a set of generalized masses, mode shapes, and natural frequencies of the model. The first 10 elastic modes were used for analysis purposes. The modes were determined using a finite-element model of the wing. The modes cover a frequency range from 5.23 Hz to 118.15 Hz. Generalized masses and frequencies are presented in table I.

Aerodynamic Properties

The aerodynamic terms appearing in equation (2) were calculated using doublet-lattice aerodynamics by a numerical method similar to that described in reference 5. To calculate the pressure distribution on an oscillating wing undergoing simple harmonic motion, the lifting surface is subdivided into an array of trapezoidal boxes arranged in strips parallel to the airstream as shown in figure 4. The lifting surface is then represented by a lattice of doublets located at the quarter-chord of each box. The downwash boundary condition is satisfied at the three-quarter-chord of each box. The downwash is computed from the slope and deflection of each structural mode. The lifting surface was divided into 210 boxes arranged in 30 streamwise strips with 7 boxes per strip. Oscillatory aerodynamic forces were calculated at eight reduced frequencies (k = 0, 0.1, 0.3, 0.5, 0.7, 0.9, 1.3, and 1.8).

Each of the aerodynamic terms was approximated in the s-plane through the use of equation (1). The β_{m-2} terms were arbitrarily selected to be 0.2, 0.4, 0.6, and 0.8, respectively. Figure 5 shows a comparison between the oscillatory

data and the approximating function for Q_{11} and Q_{22} at $M = 0.90$. These two aerodynamic terms were selected because of their importance in the flutter calculations. As indicated in figure 5, the fit is good. In general, errors in the aerodynamic forces were less than 10 percent and in most cases less than 1 percent.

Control Law

The active flutter-suppression system that was implemented on the model is illustrated in the following sketch:

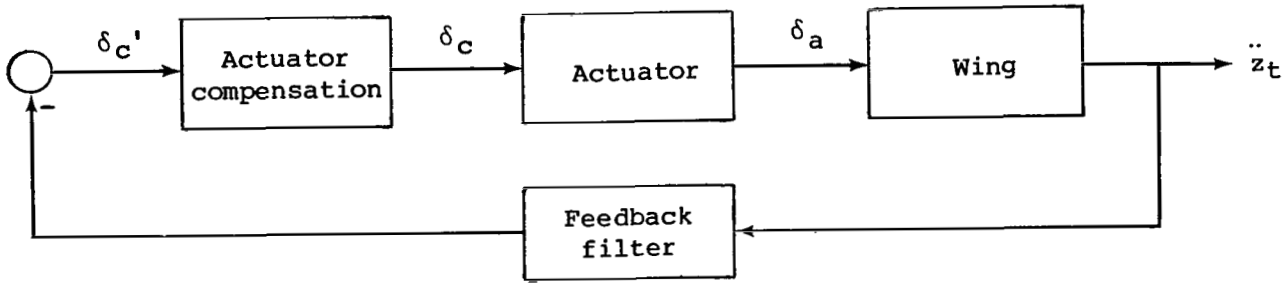

where

$$\frac{\delta_c'(s)}{s^2\, z_t(s)} = \frac{4.37 \times 10^{11} s (s^2 + D_m s + 1.169 \times 10^4)(s^2 + 22.7s + 1432)(s^2 + 216.2s + 4.675 \times 10^4)}{(s + 1.1)(s + D_m)(s + 21.6)^2 (s^2 + 43.3s + 2922)(s + 432.4)(s + 486.5)^2 (s + 628.3)^2}$$

in degrees per g unit,

$$\frac{\delta_c(s)}{\delta_c'(s)} = \frac{2.795(s^2 + 179.4s + 8.945 \times 10^4)}{(s^2 + 350s + 500^2)}$$

in degrees per degree,

$$\frac{\delta_a(s)}{\delta_c(s)} = \frac{3.057 \times 10^{13}}{(s + 214)(s^2 + 179.4s + 8.945 \times 10^4)(s^2 + 747.9s + 1.597 \times 10^6)}$$

in degrees per degree, and

$$\ddot{z}_t = \ddot{z}(x = 0.60c,\ y = 0.92L_s)$$

Therefore,

$$\frac{\delta_a(s)}{z_t(s)} = \frac{3.734 \times 10^{25} s^3 (s^2 + D_m s + 1.169 \times 10^4)(s^2 + 22.7s + 1432)(s^2 + 216.2s + 4.675 \times 10^4)}{(s + 1.1)(s + D_m)(s + 21.6)^2 (s^2 + 43.3s + 2922)(s + 432.4)(s + 486.5)^2 (s + 628.3)^2 (s^2 + 350s + 500^2)(s + 214)(s^2 + 747.9s + 1.597 \times 10^6)} \qquad (10)$$

in degrees per g unit. The control surface has a 20-percent chord and is located between span stations $y = 0.763L_s$ and $y = 0.893L_s$. Locations of the control surface and of the feedback accelerometer are shown in figure 3. The feedback filter parameter D_m varies with Mach number M and dynamic pressure q in the following manner:

$$D_m = -83.54q - 900M + 1540 \tag{11}$$

RESULTS AND DISCUSSION

Wing Without Flutter-Suppression System

The eigenvalues of equation (5) are the roots of the characteristic flutter equation for the wing without flutter suppression (system off). Since the matrix [A] varies with dynamic pressure, a root locus illustrating the variation of the flexible mode eigenvalues with dynamic pressure can be constructed for each Mach number. A typical root locus at $M = 0.90$ is given in figure 6. (It should be noted that extra roots associated with the aerodynamic poles in eq. (1) are calculated when solving for the eigenvalues of eq. (5), but are not presented in fig. 6.) Root loci for each flexible mode are indicated in the figure. Arrows indicate increasing dynamic pressure. A classical flutter behavior is apparent since the frequencies of modes 1 and 2 tend to coalesce with increasing dynamic pressure as mode 1 crosses into the unstable region. The value of dynamic pressure q at flutter is given in the figure. Calculations performed at $M = 0.60$, 0.70, and 0.80 show a similar behavior but with a more rapid degradation in damping as the flutter point is approached. This is shown by the results given in figure 7 which compare the loci of mode 1 at $M = 0.6$, 0.7, 0.8, and 0.9. The tick marks represent calculations performed at dynamic pressure increments of 0.24 kPa. The results show that as Mach number is reduced the variations in the real part of the roots near the instability are increased for the same increment in dynamic pressure. Calculated flutter dynamic pressures and frequencies are given in table II. A value of equivalent viscous damping ζ of 0.005 was assumed for all calculations.

Since modal damping is proportional to

$$\tan\left(\frac{\text{Real part of root}}{\text{Imaginary part of root}}\right)$$

the same analytical results presented as root locus plots can also be presented in the familiar form of damping and frequency versus dynamic pressure. An example of these data at $M = 0.90$ and $M = 0.60$ for modes 1 and 2 is presented in figures 8(a) and 8(b), respectively. These plots are useful in qualitatively assessing the nature of flutter onset. At $M = 0.90$ (fig. 8(a)) the damping of mode 1 is low throughout the dynamic-pressure range and the slope of the curve at flutter is not severe. These results indicate that the response in mode 1 would be quite evident and the variation in frequency could be easily monitored. Figure 8(b) shows that at $M = 0.60$ the reduction in damping above a dynamic pressure of 6.7 kPa is quite rapid, which indicates a more violent flutter onset. These qualitative results were confirmed during tunnel tests.

System-off experimental flutter points were measured at $M = 0.6$, 0.8, and 0.9. Figure 9 presents a comparison of the predicted and measured flutter dynamic pressures and frequencies. Measured dynamic pressures and frequencies are given in table II. The results show good agreement at all Mach numbers.

Wing With Active Flutter-Suppression System

The eigenvalues of equation (9) are the roots of the characteristic equation for the wing with active flutter suppression (system on). Root locus plots at $M = 0.90$ and $M = 0.60$ are presented in figures 10 and 11. Root loci for each flexible mode and for the two filter modes introduced by the denominator terms (see eq. (10)) $(s + 21.6)^2$ and $(s^2 + 43.3s + 2922)$ are given in each figure. (It should be noted that the equations were solved with the complete transfer function defined by eq. (10). However, only the results of the 10 flexible modes and the 2 filter modes are presented in figs. 10 and 11.) At $M = 0.90$ an instability at a dynamic pressure of 9.289 kPa results from a coupling between the first structural mode and the filter mode $(s + 21.6)^2$. An 84.8-percent increase in flutter dynamic pressure over that of the wing without flutter suppression is predicted. Calculations performed at $M = 0.7$ and 0.8 (not shown) predict the same type of behavior with increases in flutter dynamic pressure of 68 percent and 60 percent, respectively. Calculations at $M = 0.60$ (fig. 11) show a different behavior with the first flexible mode going unstable at a dynamic pressure of 9.337 kPa. This probably occurs because as Mach number decreases the system-off flutter frequency increases, which results in a decoupling between the first wing mode and the filter mode. Calculated system-on instability dynamic pressures and frequencies are given in table II. All system-on calculations include scheduling of the filter parameter D_m as given by equation (11).

System-on tests above the system-off wing flutter boundary were performed only at $M = 0.90$. Figure 12 presents a summary of the predicted and measured effect of the flutter-suppression system. The model was stable to approximately 42 percent above the system-off flutter boundary. At this point, the control-system-commanded aileron displacement exceeded that available on the model ($\delta_{a,max} = \pm 14^\circ$) and the system saturated, which resulted in an instability. The frequency of the instability was approximately 8.5 Hz, which indicated a complete loss in effectiveness of the flutter-suppression system when the saturation occurred. System-on tests at $M = 0.8$ and $M = 0.6$ were performed below the system-off wing flutter boundary. In all cases the wing was stable and the response of the wing to tunnel turbulence was reduced with the flutter-suppression system operating.

It is believed that the saturation and resulting instability experienced on the model was a result of tunnel turbulence. Unpublished data taken from measurements of pressure fluctuations in the transonic dynamics tunnel indicate that the largest pressure peaks occur in the 8 to 15 Hz frequency range at Mach numbers between 0.87 and 0.95. At $M = 0.90$ and $q = 7.59$ kPa, equations (10) and (11) predict a control-surface displacement of approximately 11° per g unit for motion in the first flexible mode. At this test point accelerations in the frequency range of the first flexible mode were in excess of 1.6g. It can

therefore be assumed that the turbulence input to the model is greatest in the frequency range of the first mode and this led to large control-surface motions and finally to saturation. Prior to the instability, control-surface commands in excess of 20° were recorded. Reference 6 points out the need to consider stability and turbulence criteria simultaneously when designing a flutter-suppression system.

In an effort to predict these results analytically, a gust calculation was performed on the wind-tunnel model using the methods described in appendix B. However, the power spectral density of the wind-tunnel turbulence is not modeled properly using a Von Kármán gust spectrum. During the calculations the characteristic length of the Von Kármán spectrum was varied to match the root-mean-square (rms) deflection of the control surface at the saturation point ($M = 0.9$; $q = 7.59$ kPa). The measured and predicted variation in rms control deflection is given in figure 13. A gust intensity of 0.3048 m/sec was assumed for all calculations. The effect of reducing the gust length is to increase the gust input power at the first mode frequency.

Since the design of a flutter-suppression system depends on both stability and response to turbulence, some effort to adequately model the tunnel turbulence is necessary if meaningful results are to be obtained. This study is beyond the scope of the present investigation.

CONCLUSIONS

An analytical method for predicting the increase in stability provided by an active flutter-suppression system has been presented. The method is based on approximating the unsteady aerodynamic forces in the time plane through an interpolating function in the frequency plane. The analytical method is applied to an aeroelastic model equipped with an active flutter-suppression system that was tested in the Langley transonic dynamics tunnel. Some of the important conclusions are:

(1) The analytical technique presented provides a convenient method for adding active control systems to the equations of motion.

(2) The use of interpolating functions to approximate the unsteady aerodynamics provides a good prediction of the flutter characteristics of the wing without flutter suppression at all Mach numbers investigated.

(3) Analytical results predict an 84.8-percent increase in the flutter dynamic pressure for the wing with flutter suppression at $M = 0.90$. Experimental results demonstrate a 42-percent increase prior to control-system saturation.

(4) Results of this study indicate the need for a more adequate model of wind-tunnel turbulence before a thorough evaluation of the analytical techniques can be performed for the wing with active flutter suppression.

Langley Research Center
National Aeronautics and Space Administration
Hampton, VA 23665
December 22, 1978

APPENDIX A

AERODYNAMIC APPROXIMATION

Three-dimensional unsteady forces are normally computed at a given Mach number for simple harmonic motion at specific values of reduced frequency k. The transfer function which relates control-surface motion to wing response is normally expressed as a ratio of polynomials in the variable s. This appendix describes a technique, similar to that described in reference 3, which permits the variation of the aerodynamic forces with reduced frequency to be approximated by a rational polynomial in s.

Consider the function

$$\hat{Q}(k) = A_0 + A_1(jk) + A_2(jk)^2 + \sum_{m=3}^{6} \frac{A_m(jk)}{(jk + \beta_{m-2})} \tag{A1}$$

to be an approximate fit to Q. The real and imaginary parts of Q are

$$\left.\begin{aligned} Q_R &= A_0 - A_2k^2 + \frac{k^2A_3}{k^2 + \beta_1^2} + \frac{k^2A_4}{k^2 + \beta_2^2} + \frac{k^2A_5}{k^2 + \beta_3^2} + \frac{k^2A_6}{k^2 + \beta_4^2} \\ Q_I &= A_1k + \frac{\beta_1kA_3}{k^2 + \beta_1^2} + \frac{\beta_2kA_4}{k^2 + \beta_2^2} + \frac{\beta_3kA_5}{k^2 + \beta_3^2} + \frac{\beta_4kA_6}{k^2 + \beta_4^2} \end{aligned}\right\} \tag{A2}$$

Q is calculated at discrete values of reduced frequency k. At each value of reduced frequency real and imaginary error functions are determined from equations (A2); that is

$$\left.\begin{aligned} E_{R,i} &= Q_{R,i} + [B_{R,i}]\{C\} \\ E_{I,i} &= Q_{I,i} + [B_{I,i}]\{C\} \end{aligned}\right\} \tag{A3}$$

where

$$[B_{R,i}] = \left[-1 \quad 0 \quad k_i^2 \quad \frac{-k_i^2}{k_i^2 + \beta_1^2} \quad \frac{-k_i^2}{k_i^2 + \beta_2^2} \quad \frac{-k_i^2}{k_i^2 + \beta_3^2} \quad \frac{-k_i^2}{k_i^2 + \beta_4^2}\right]$$

$$[B_{I,i}] = \left[0 \quad -k_i \quad 0 \quad \frac{-\beta_1k_i}{k_i^2 + \beta_1^2} \quad \frac{-\beta_2k_i}{k_i^2 + \beta_2^2} \quad \frac{-\beta_3k_i}{k_i^2 + \beta_3^2} \quad \frac{-\beta_4k_i}{k_i^2 + \beta_4^2}\right]$$

APPENDIX A

$$\{C\} = \begin{Bmatrix} A_0 \\ A_1 \\ \cdot \\ \cdot \\ \cdot \\ A_6 \end{Bmatrix}$$

and i refers to a particular reduced frequency k_i at which Q is calculated. Defining a complex error function as

$$E_i = E_{R,i} + jE_{I,i}$$

a least-squares fit can be passed through the N data points by setting

$$\frac{\partial}{\partial c} \sum_{i=1}^{N} (E_i \times E_i^*) = 0$$

Where E_i^* is the complex conjugate of E_i. Performing this differentiation results in the following set of normal equations

$$\sum_{i=1}^{N} \left(Q_{R,i} + [B_{R,i}]\{C\}\right)\{B_{R,i}\} + \left(Q_{I,i} + [B_{I,i}]\{C\}\right)\{B_{I,i}\} = 0$$

which can be solved for the coefficients of the fit. That is,

$$\{C\} = -\left[\sum_{i=1}^{N}\left(\{B_{R,i}\}[B_{R,i}] + \{B_{I,i}\}[B_{I,i}]\right)\right]^{-1} \sum_{i=1}^{N} \left(Q_{R,i}\{B_{R,i}\} + Q_{I,i}\{B_{I,i}\}\right) \qquad \text{(A4)}$$

Since $k = \omega b/V$, let $s = j\omega$ and $jk = s(b/V)$. Substituting this relationship into equation (A1) results in

$$\hat{Q}(s) = A_0 + A_1\left(\frac{b}{V}\right)s + A_2\left(\frac{b}{V}\right)^2 s^2 + \sum_{m=3}^{6} \frac{A_m s}{\left(s + \frac{V}{b}\beta_{m-2}\right)} \qquad \text{(A5)}$$

where the coefficients $A_0, A_1, \ldots, A_6$ are determined from equation (A4). The values of β_{m-2} are arbitrarily selected from the range of reduced frequencies for which Q has been calculated.

As described in reference 3, the form of equation (A5) permits an approximation of the time delays inherent in unsteady aerodynamics subject to the

following requirements: complex conjugate symmetry, denominator roots in the left-half plane, and a good approximation of the complex aerodynamic forces at $s = j\omega$. The form of equation (A5) is used to fit all of the wing motion, control surface, and gust unsteady aerodynamic forces.

APPENDIX B

FORMULATION OF EQUATIONS OF MOTION FOR STABILITY AND GUST ANALYSIS

The equations of motion are formulated in terms of real matrices by using an "approximation function" for the complex aerodynamic forces. The variation with s of the aerodynamic matrix $[\hat{Q}]$ is given as (see appendix A)

$$[\hat{Q}] = [A_0] + [A_1]\left(\frac{b}{V}\right)s + [A_2]\left(\frac{b}{V}\right)^2 s^2 + \sum_{m=3}^{6} \frac{[A_m]s}{\left(s + \frac{V}{b}\beta_{m-2}\right)}$$

After substituting $[\hat{Q}]$ for $\mathcal{L}\left([Q]\right)$ in equation (4), the equation of motion may be written as

$$\left([M]s^2 + [2\zeta_M\omega_n]s + \frac{1}{2}\rho V^2[\hat{Q}] + [K]\right)\{\bar{q}\} = \{\hat{F}_G\} \tag{B1}$$

These are the equations for n structural modes with r active controls where $[M]$ represents the mass matrix, $[K]$ the stiffness matrix, ρ the fluid density, V the fluid velocity, $\{\hat{F}_G\}$ the aerodynamic gust force, and $\{\bar{q}\}$ the response vector. All the matrices in equation (B1) are of the size $n \times (n + r)$.

Flutter Analysis - No Controls

Substituting the aerodynamic approximating coefficients into equation (B1) with $\{\hat{F}_G\} = 0$, the equations of motion in terms of real matrices are written as

$$\left[s^2[M] + [2\zeta_M\omega_n]s + [K]\right]\{q\} + \frac{1}{2}\rho V^2\left[s^2\left(\frac{b}{V}\right)^2[A_2]\right.$$

$$\left. + s\left(\frac{b}{V}\right)[A_1] + [A_0] + \sum_{m=3}^{6} \frac{[A_m]s}{\left(s + \frac{V}{b}\beta_{m-2}\right)}\right]\{q\} = 0 \tag{B2}$$

where $\{\bar{q}\} = \{q\}$ for the no-control case. The matrices in equation (B2) are

of the size $n \times n$. Multiplying through by the denominator term yields a polynomial in s of the form

$$\left(A_0(s)\left[[\bar{A}]s^2 + [\bar{B}]s + [\bar{C}]\right] + A_1(s)[\bar{D}] + A_2(s)[\bar{E}] + A_3(s)[\bar{F}] + A_4(s)[\bar{G}]\right)\{q\} = 0 \tag{B3}$$

where

$$A_0(s) = \left(s + \frac{V}{b}\beta_1\right)\left(s + \frac{V}{b}\beta_2\right)\left(s + \frac{V}{b}\beta_3\right)\left(s + \frac{V}{b}\beta_4\right)$$

$$A_1(s) = s\left(s + \frac{V}{b}\beta_2\right)\left(s + \frac{V}{b}\beta_3\right)\left(s + \frac{V}{b}\beta_4\right)$$

$$A_2(s) = s\left(s + \frac{V}{b}\beta_1\right)\left(s + \frac{V}{b}\beta_3\right)\left(s + \frac{V}{b}\beta_4\right)$$

$$A_3(s) = s\left(s + \frac{V}{b}\beta_1\right)\left(s + \frac{V}{b}\beta_2\right)\left(s + \frac{V}{b}\beta_4\right)$$

$$A_4(s) = s\left(s + \frac{V}{b}\beta_1\right)\left(s + \frac{V}{b}\beta_2\right)\left(s + \frac{V}{b}\beta_3\right)$$

$$[\bar{A}] = [M] + \frac{1}{2}\rho b^2[A_2]$$

$$[\bar{B}] = \frac{1}{2}\rho V b[A_1] + [2\zeta M\omega_n]$$

$$[\bar{C}] = \frac{1}{2}\rho V^2[A_0] + [K]$$

$$[\bar{D}] = \frac{1}{2}\rho V^2[A_3]$$

$$[\bar{E}] = \frac{1}{2}\rho V^2[A_4]$$

$$[\bar{F}] = \frac{1}{2}\rho V^2 [A_5]$$

$$[\bar{G}] = \frac{1}{2}\rho V^2 [A_6]$$

After the indicated polynomial products are performed, equations (B3) can be written as

$$\left([F_6]s^6 + [F_5]s^5 + \ldots + [F_0]\right)\{q\} = 0 \tag{B4}$$

The matrix coefficients $[F_i]$ $(i = 0, 1, \ldots, 6)$ are functions of dynamic pressure and velocity for a given Mach number. By using the relationships that

$$\{X\} = \begin{Bmatrix} s^5\{q\} \\ s^4\{q\} \\ \vdots \\ s^0\{q\} \end{Bmatrix}$$

equation (B4) can be reduced to the following 6n first-order equations:

$$s\{X\} = [A]\{X\} \tag{B5}$$

where

$$[A] = \begin{bmatrix} [-F_6^{-1}F_5] & [-F_6^{-1}F_4] & \ldots & [-F_6^{-1}F_0] \\ [I] & 0 & \ldots & 0 \\ 0 & [I] & \ldots & 0 \\ \vdots & \vdots & \vdots & \vdots \\ 0 & 0 & [I] & 0 \end{bmatrix} \tag{B6}$$

APPENDIX B

The matrix [A] is $6n \times 6n$. For a fixed value of Mach number, dynamic pressure, and velocity, the eigenvalues of equation (B6) are the roots of the characteristic flutter equation. Since the matrix elements $[F_i]$ are functions of dynamic pressure (for a constant Mach number), the loci of roots as a function of dynamic pressure can be constructed.[1] These loci correspond to the variation in the eigenvalues of each flexible mode as dynamic pressure is varied at a constant Mach number.

Stability Analysis - With Controls

For the case of r controls, the response vector $\{\bar{q}\}$ can be expressed in terms of n structural modes and r control deflections as

$$\{\bar{q}\} = \begin{Bmatrix} q \\ q_c \end{Bmatrix}$$

Equation (B1), with $\{\hat{F}_G\} = 0$, can be written as

$$\left(\left[M \mid M_c \right] s^2 + \left[2\zeta M \omega_n \mid 0 \right] s + \frac{1}{2}\rho V^2 \left[\hat{Q} \mid \hat{Q}_c \right] + \left[K \mid K_c \right] \right) \begin{Bmatrix} q \\ q_c \end{Bmatrix} = 0 \tag{B7}$$

where the subscript c denotes a control quantity. The control law relates control-surface motion to wing response and can be written in the form

$$\{q_c\} = [T]\{z_t\} \tag{B8}$$

where $\{z_t\}$ are the values of wing response at the sensor location. The response $\{z_t\}$ can be written in terms of modal response by

$$\{z_t\} = [\phi_t]\{q\}$$

where $[\phi_t]$ is the matrix of modal deflections at the sensor locations. Therefore,

$$\{q_c\} = [T][\phi_t]\{q\}$$

---

[1]For a given Mach number, the flight velocity V varies somewhat because of the change in speed of sound with altitude. For a wind-tunnel model, Mach number fixes the value of V.

APPENDIX B

Typically, the transfer function matrix [T] is expressed as a rotational polynomial in s. Therefore, let

$$[T] = \frac{[T_N]}{D(s)} \tag{B9}$$

where D(s) is a polynomial representing the common denominator of all the [T] terms, and $[T_N]$ is a matrix of the resulting numerators. (For the example in the text, $T_N = s^2N(s)$.) Substituting equations (B9) and (B8) into (B7) results in the following equation of motion:

$$\left[s^2[M] + s[2\zeta M\omega_n] + [K]\right]\{q\} + \frac{1}{2}\rho V^2\left[s^2\left(\frac{b}{V}\right)^2[A_2] + s\left(\frac{b}{V}\right)[A_1] + [A_0] \right.$$

$$\left. + \sum_{m=3}^{6} \frac{[A_m]s}{\left(s + \frac{V}{b}\beta_{m-2}\right)} \right]\{q\} + \left[s^2[M_c] + [K_c] + \frac{1}{2}\rho V^2\left[s^2\left(\frac{b}{V}\right)^2\left[A_2, q_c\right] + s\left(\frac{b}{V}\right) \right.\right.$$

$$\left.\left. \times \left[A_1, q_c\right] + \left[A_0, q_c\right] + \sum_{m=3}^{6} \frac{\left[A_m, q_c\right]s}{\left(s + \frac{V}{b}\beta_{m-2}\right)} \right] \right] \frac{[T_N][\phi_t]\{q\}}{D(s)} = 0$$

where the values of $\left[A_i, q_c\right]$ (i = 0, 1, . . ., 6) are the aerodynamic matrix coefficients for each control surface. Multiplying through by the denominator term yields a polynomial in s of the form

$$\left[D(s)\left(A_0(s)\left[[\bar{A}]s^2 + [\bar{B}]s + [\bar{C}]\right] + A_1(s)[\bar{D}] + A_2(s)[\bar{E}] + A_3(s)[\bar{F}] + A_4(s)[\bar{G}]\right) \right.$$

$$+ \left(A_0(s)\left[[\bar{A}_c]s^2 + [\bar{B}_c]s + [\bar{C}_c]\right] + A_1(s)[\bar{D}_c] + A_2(s)[\bar{E}_c] + A_3(s)[\bar{F}_c] + A_4(s)[\bar{G}_c]\right)$$

$$\left. \times [T_N][\phi_t] \right]\{q\} = 0 \tag{B10}$$

where

$$[\bar{A}_c] = \frac{1}{2}\rho b^2\left[A_2, q_c\right] + [M_c]$$

$$[\bar{B}_c] = \frac{1}{2}\rho b\left[A_1, q_c\right]$$

$$[\bar{C}_c] = \frac{1}{2}\rho V^2\left[A_0, q_c\right] + [K_c]$$

$$[\bar{D}_c] = \frac{1}{2}\rho V^2\left[A_3, q_c\right]$$

$$[\bar{E}_c] = \frac{1}{2}\rho V^2\left[A_4, q_c\right]$$

$$[\bar{F}_c] = \frac{1}{2}\rho V^2\left[A_5, q_c\right]$$

$$[\bar{G}_c] = \frac{1}{2}\rho V^2\left[A_6, q_c\right]$$

Equation (B10) can be written as

$$\left([F_m]s^m + [F_{m-1}]s^{m-1} + \ldots + [F_0]\right)\{q\} = 0$$

where $m = 6$ + highest order of polynomial $D(s)$. In a manner similar to that discussed in the previous section this equation can be reduced to a series of first-order equations of the following form:

$$s\{X\} = [A_c]\{X\} \tag{B11}$$

where

$$\{X\} = \begin{Bmatrix} s^{m-1}\{q\} \\ s^{m-2}\{q\} \\ \vdots \\ s^0\{q\} \end{Bmatrix}$$

and

$$[A_C] = \begin{bmatrix} \left[-F_m^{-1}F_{m-1}\right] & \left[-F_m^{-1}F_{m-2}\right] & \cdots & \left[-F_m^{-1}F_0\right] \\ [I] & 0 & \cdots & 0 \\ 0 & [I] & \cdots & 0 \\ \vdots & \vdots & \vdots & \vdots \\ 0 & 0 & [I] & 0 \end{bmatrix} \tag{B12}$$

The matrix $[A_C]$ is $mn \times mn$. For a fixed value of Mach number, dynamic pressure, and velocity, the eigenvalues of equation (B12) are the roots of the characteristic equation. Root loci can now be constructed which correspond to the variation in the eigenvalues of the system as dynamic pressure is varied.

Gust Analysis - With Controls

The gust response analysis is performed using power-spectral-density (PSD) techniques similar to those described in reference 7. Equation (B1) permits the direct evaluation of the system response to a sinusoidally varying gust. The term $\{\hat{F}_G\}$ in equation (B1) is defined as

$$\{\hat{F}_G\} = -\frac{1}{2}\rho V\left[\{A_{0,g}\} + \left(\frac{b}{V}\right)\{A_{1,g}\}s + \left(\frac{b}{V}\right)^2\{A_{2,g}\}s^2 + \sum_{m=3}^{6}\frac{\{A_{m,g}\}s}{\left(s + \frac{V}{b}\beta_{m-2}\right)}\right]w_g$$

The modal response of the system with controls per unit gust velocity can be determined by solving the following set of simultaneous equations at discrete values of s (where $s = j\omega$). In this context the aerodynamic approximation is used only to interpolate data between calculated values of reduced frequency

$$[\text{Equation (B10)}]\ \frac{\{q\}}{w_g} = D(s)\left[A_0(s)\left[\{\bar{A}_{0,g}\} + \{\bar{A}_{1,g}\}s + \{\bar{A}_{2,g}\}s^2\right] + A_1(s)\{\bar{A}_{3,g}\} + A_2(s)\{\bar{A}_{4,g}\} + A_3(s)\{\bar{A}_{5,g}\} + A_4(s)\{\bar{A}_{6,g}\}\right] \tag{B13}$$

where

$$\{\bar{A}_{0,g}\} = -\frac{1}{2}\rho V\{A_{0,g}\}$$

$$\{\bar{A}_{1,g}\} = -\frac{1}{2}\rho b\{A_{1,g}\}$$

$$\{\bar{A}_{2,g}\} = -\frac{1}{2}\rho \frac{b^2}{V}\{A_{2,g}\}$$

$$\{\bar{A}_{3,g}\} = -\frac{1}{2}\rho V\{A_{3,g}\}$$

$$\{\bar{A}_{4,g}\} = -\frac{1}{2}\rho V\{A_{4,g}\}$$

$$\{\bar{A}_{5,g}\} = -\frac{1}{2}\rho V\{A_{5,g}\}$$

$$\{\bar{A}_{6,g}\} = -\frac{1}{2}\rho V\{A_{6,g}\}$$

and $\{A_{i,g}\}$ $i = 0, 1, \ldots, 6$ are the aerodynamic matrix coefficients for a sinusoidal gust. The control-surface transfer function can then be evaluated by

$$\frac{\{q_c\}}{w_g} = \frac{[T_N][\phi_t]}{D(s)} \frac{\{q\}}{w_g} \tag{B14}$$

The power-spectral-density (PSD) values of control-surface motion are determined by evaluating

$$\phi_0(\omega) = \phi_I(\omega) \left|H(\omega)\right|^2$$

where

$H(\omega)$ = Control-surface frequency-response function described by equation (B14)

$\phi_I(\omega)$ = Von Kármán PSD gust spectrum defined by

$$\frac{L\left(1 + 8(1.339L\omega/V)^{2/3}\right)}{\pi V\left[1 + (1.339L\omega/V)^{2}\right]^{11/6}}$$

The root-mean-square (rms) value of control-surface motion per unit rms gust velocity σ_{w_g} is defined by

$$\left(\frac{\{q_c\}}{\sigma_{w_g}}\right)_{rms} = \left\{\left(\int_0^\infty \phi_0(\omega)\ d\omega\right)^{1/2}\right\} \tag{B15}$$

REFERENCES

1. Edwards, John William: Unsteady Aerodynamic Modeling and Active Aeroelastic Control. SUDAAR 504 (NASA Grant NGL-05-020-007), Stanford Univ., Feb. 1977. (Available as NASA CR-148019.)

2. Vepa, Ranjan: On the Use of Pade Approximants to Represent Unsteady Aerodynamic Loads for Arbitrarily Small Motions of Wings. AIAA Paper No. 76-17, Jan. 1976.

3. Sevart, Francis D.: Development of Active Flutter Suppression Wind Tunnel Testing Technology. AFFDL-TR-74-126, U.S. Air Force, Jan. 1975.

4. Roger, Kenneth L.: Airplane Math Modeling Methods for Active Control Design. Structural Aspects of Active Controls, AGARD-CP-228, Aug. 1977, pp. 4-1 - 4-11.

5. Albano, Edward; and Rodden, William P.: A Doublet-Lattice Method for Calculating Lift Distributions on Oscillating Surfaces in Subsonic Flows. AIAA J., vol. 7, no. 2, Feb. 1969, pp. 279-285; Errata, vol. 7, no. 11, Nov. 1969, p. 2192.

6. Nissim, E.; and Abel, I.: Development and Application of an Optimization Procedure for Flutter Suppression Using the Aerodynamic Energy Concept. NASA TP-1137, 1978.

7. Pratt, Kermit G.: Response of Flexible Airplanes to Atmospheric Turbulence. Performance and Dynamics of Aerospace Vehicles, NASA SP-258, 1971, pp. 439-503.

TABLE I.- FREQUENCY, GENERALIZED MASS, AND MODAL DEFLECTION DATA

Mode	Natural frequency, Hz	Generalized mass, kg	Modal deflection at sensor location
1	5.233	3.678	0.9228
2	19.129	7.769	-.6361
3	20.906	7.044	-.0002
4	25.769	2.970	.3450
5	46.110	4.714	.1760
6	61.234	4.758	.2356
7	79.682	5.156	.0199
8	86.030	11.297	.0002
9	98.087	7.558	.0438
10	118.150	5.501	.0172

TABLE II.- SUMMARY OF RESULTS

Mach number	Wing without flutter suppression				Wing with flutter suppression			
	Analysis		Experiment		Analysis		Experiment	
	q, kPa	Frequency, Hz	q, kPa	Frequency, Hz	q, kPa	Frequency, Hz	q, kPa	Frequency, Hz
0.9	5.027	8.1	5.36	8.0	9.289	4.1	(a)	---
.8	6.033	8.9	6.08	8.6	10.128	4.2	---	---
.7	6.799	9.6	----	----	10.896	4.0	---	---
.6	7.374	10.3	7.25	10.1	9.337	7.6	---	---

[a]No flutter to q = 7.590 kPa.

○ ijth calculated unsteady aerodynamic force [Q] at discrete values of k

□ ijth approximation to unsteady aerodynamic force [$\hat{Q}$] at $s = j\frac{kV}{b}$

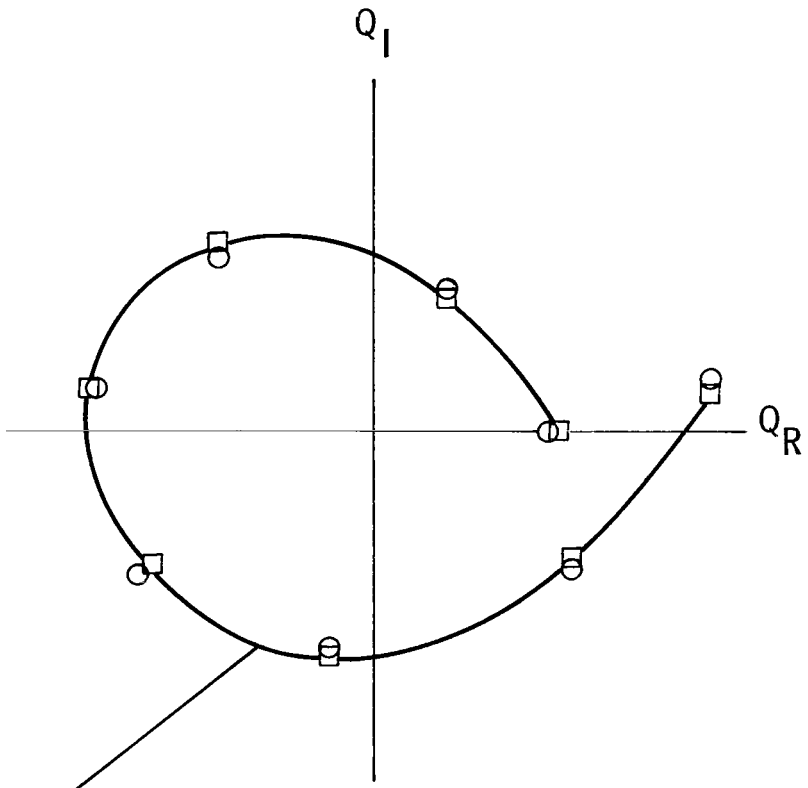

$$\hat{Q}(s) = A_0 + A_1\left(\frac{b}{V}\right)s + A_2\left(\frac{b}{V}\right)^2 s^2 + \sum_{m=3}^{6} \frac{A_m s}{\left(s + \frac{V}{b}\beta_{m-2}\right)}$$

Figure 1.- Typical fit of a complex aerodynamic force.

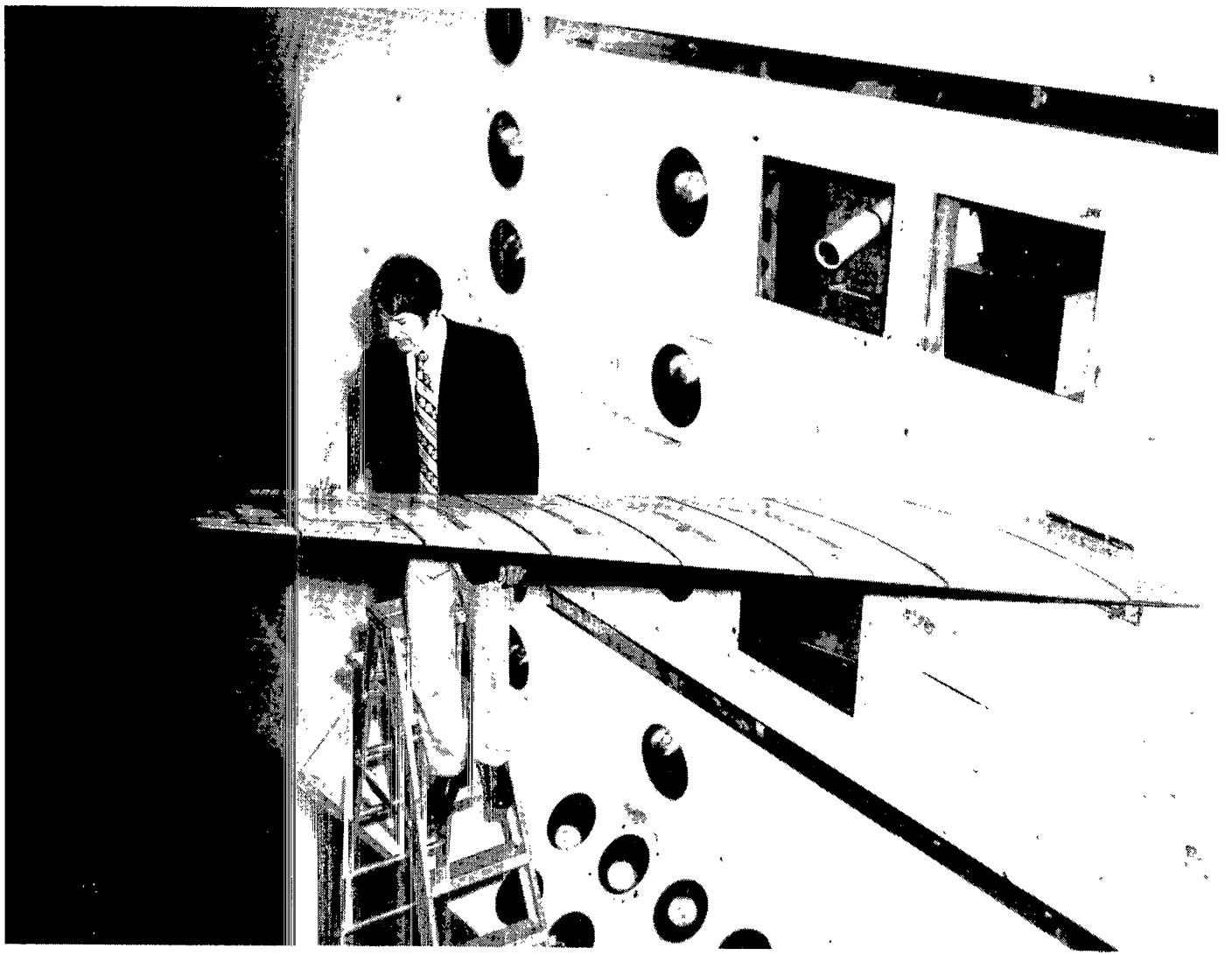

L-78-976

Figure 2.- Flutter-suppression model mounted in the Langley transonic dynamics tunnel.

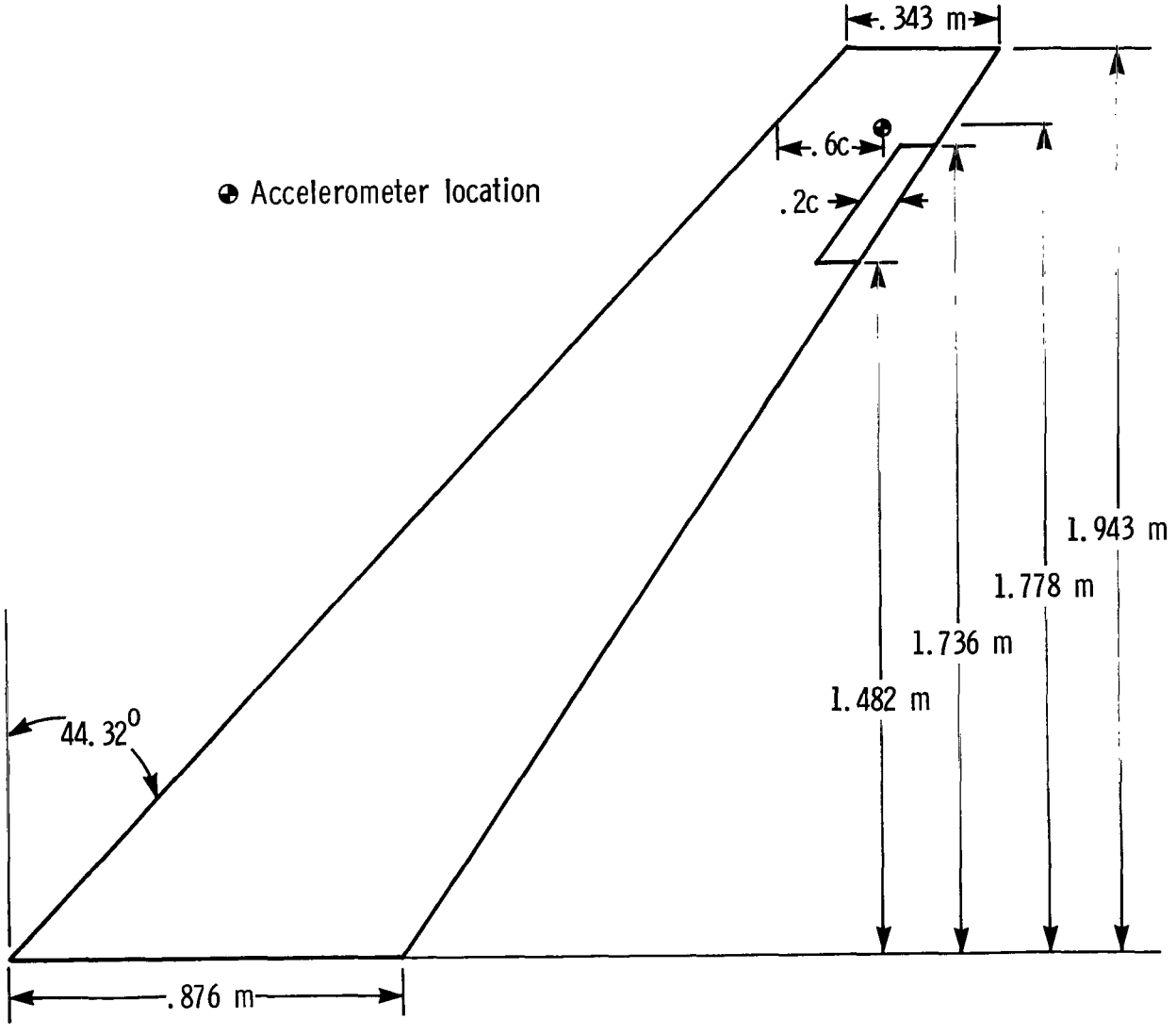

Figure 3.- Model geometry.

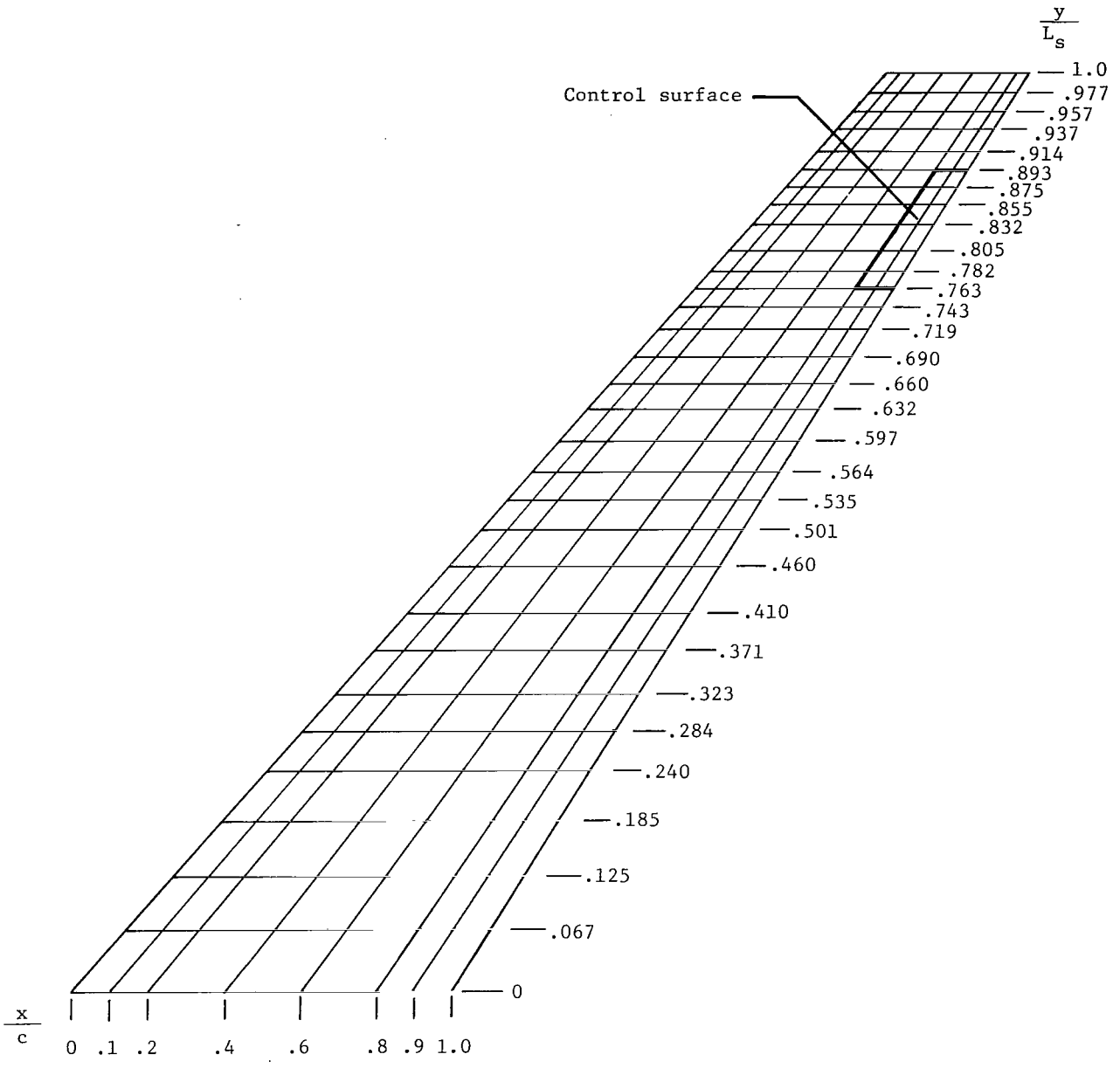

Figure 4.- Paneling scheme for doublet-lattice aerodynamics.

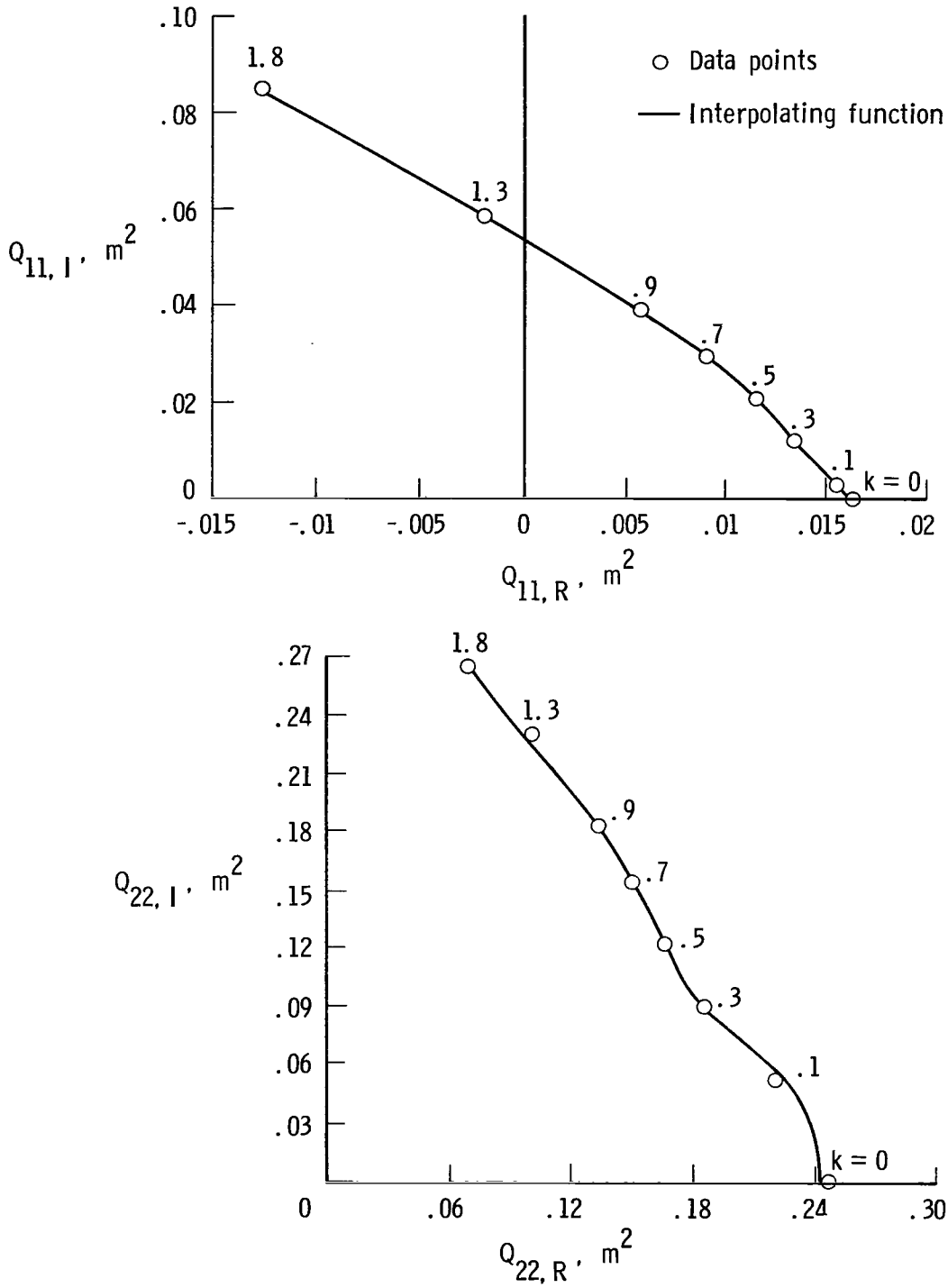

Figure 5.- Aerodynamic curve fit for Q_{11} and Q_{22} at M = 0.90.

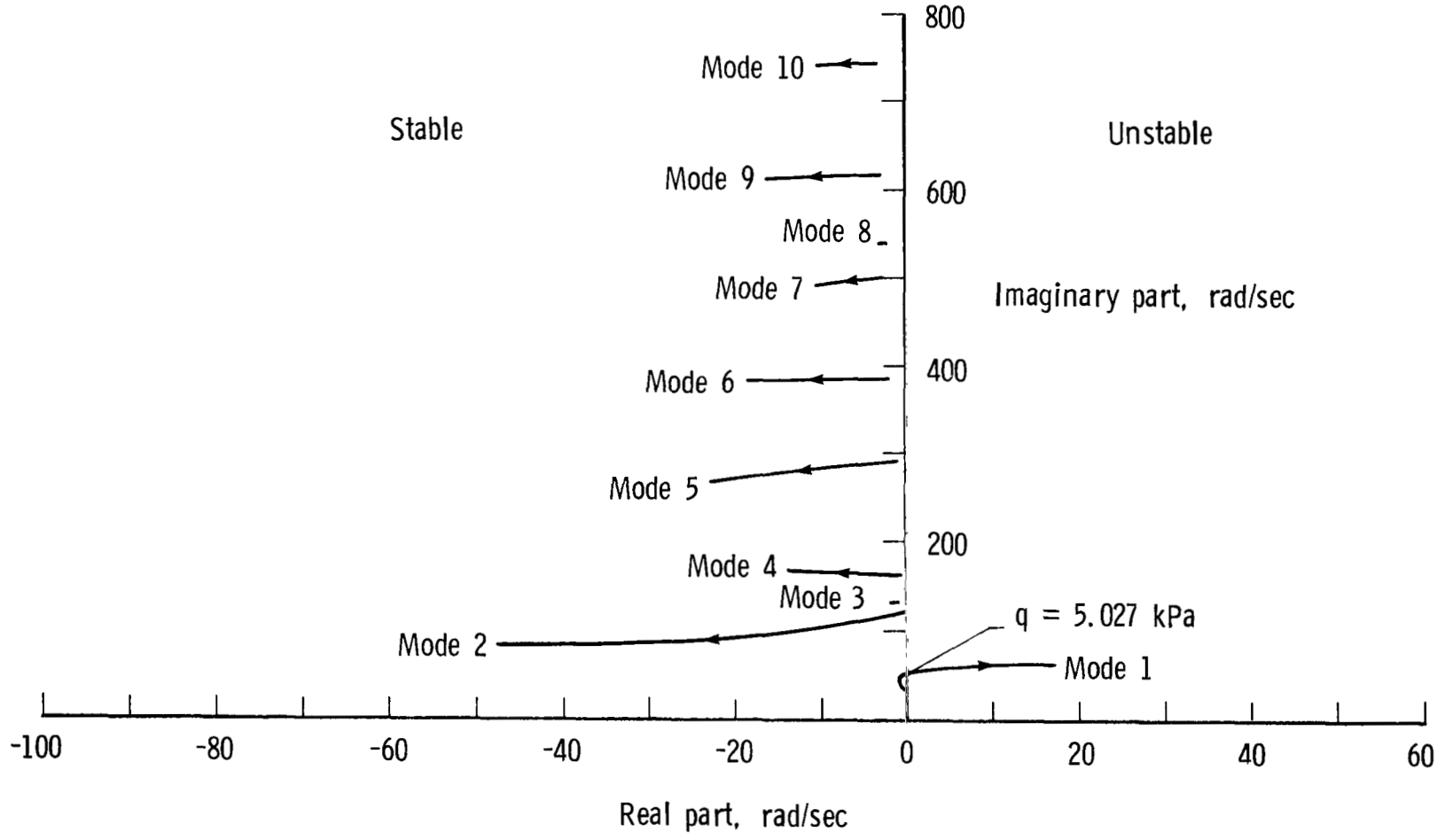

Figure 6.- Dynamic-pressure root locus at M = 0.90 (system off). Arrows indicate increasing dynamic pressure.

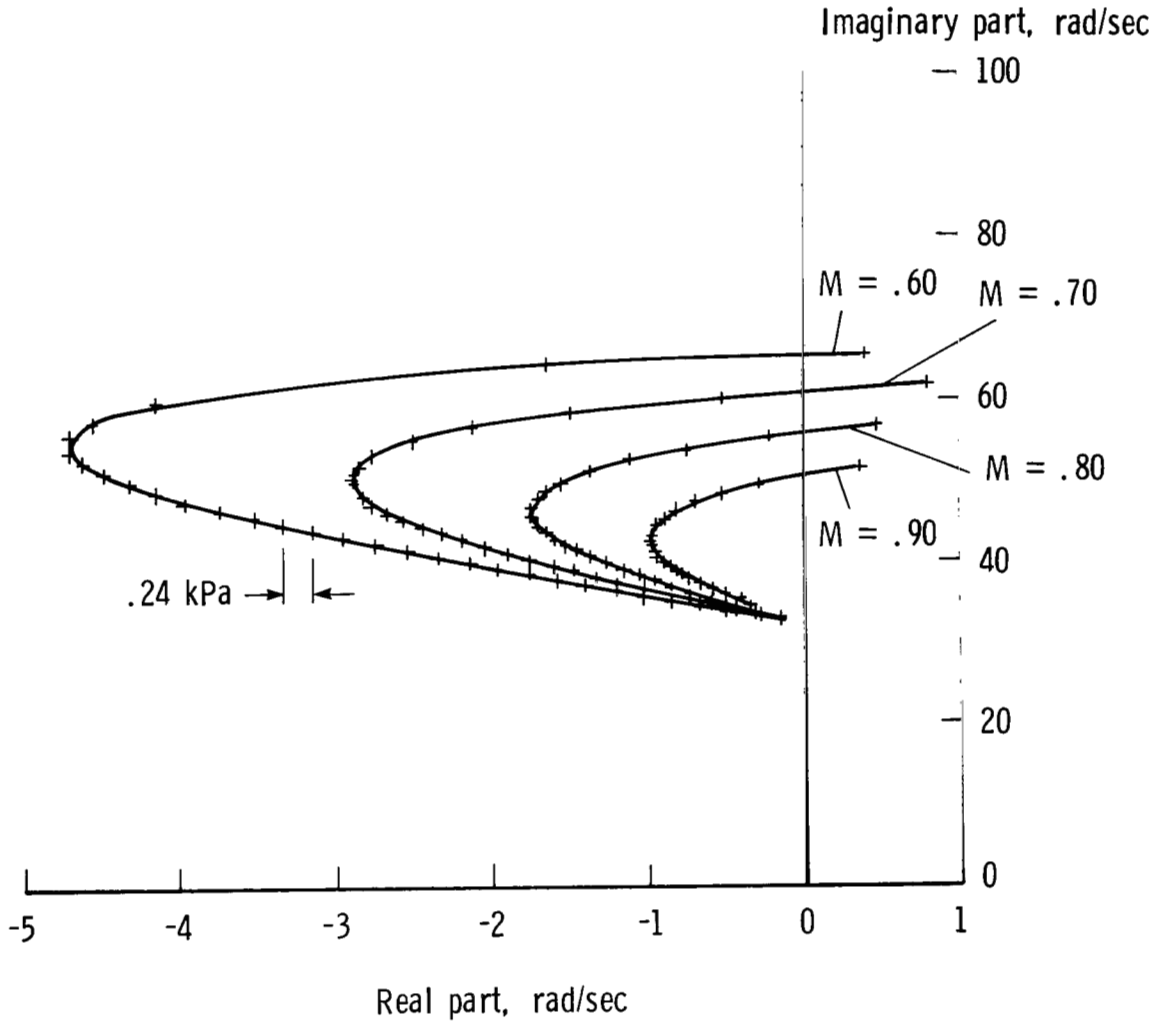

Figure 7.- Root loci of mode 1 as a function of Mach number and dynamic pressure (system off).

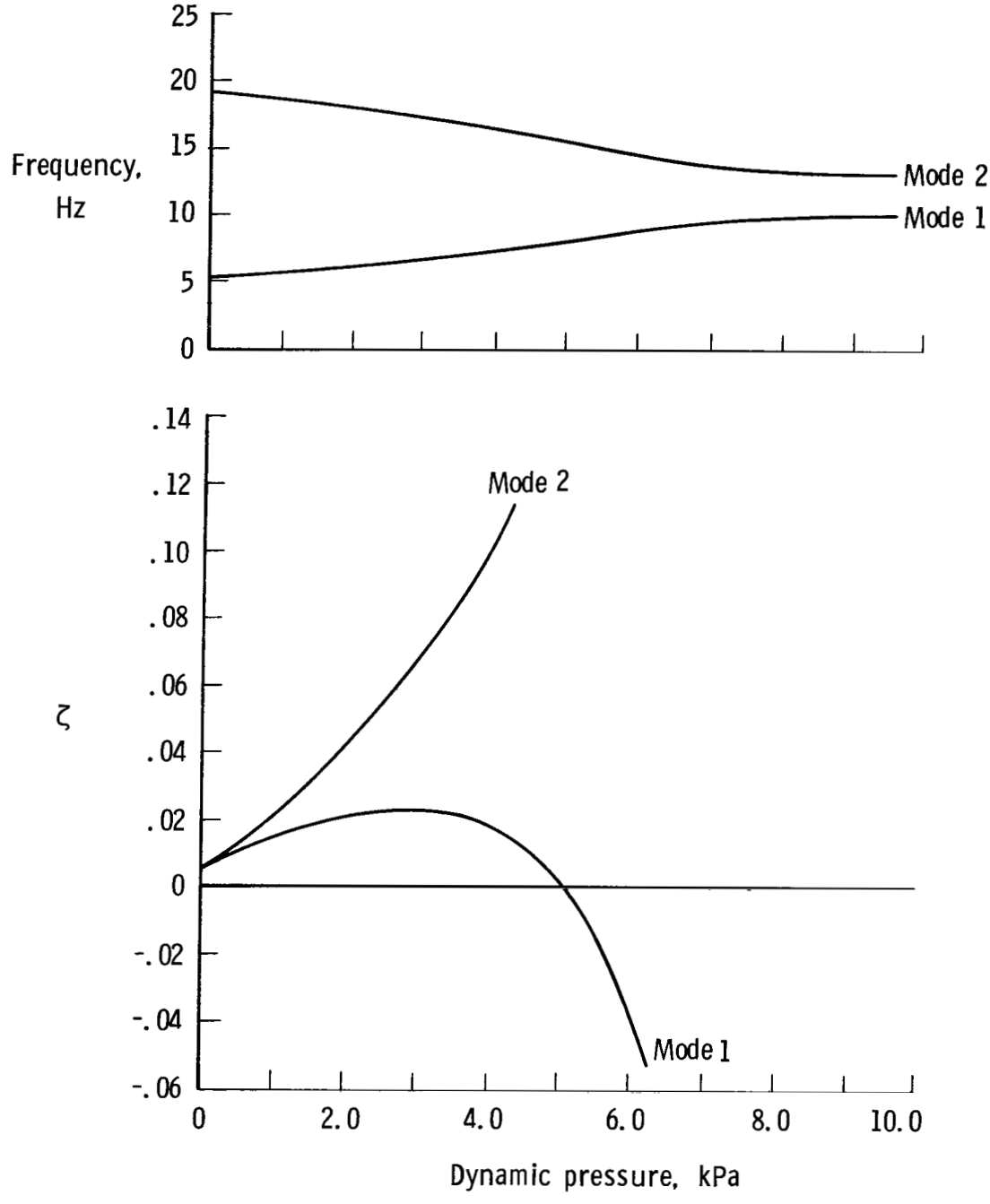

(a) M = 0.90.

Figure 8.- Damping and frequency versus dynamic pressure (system off).

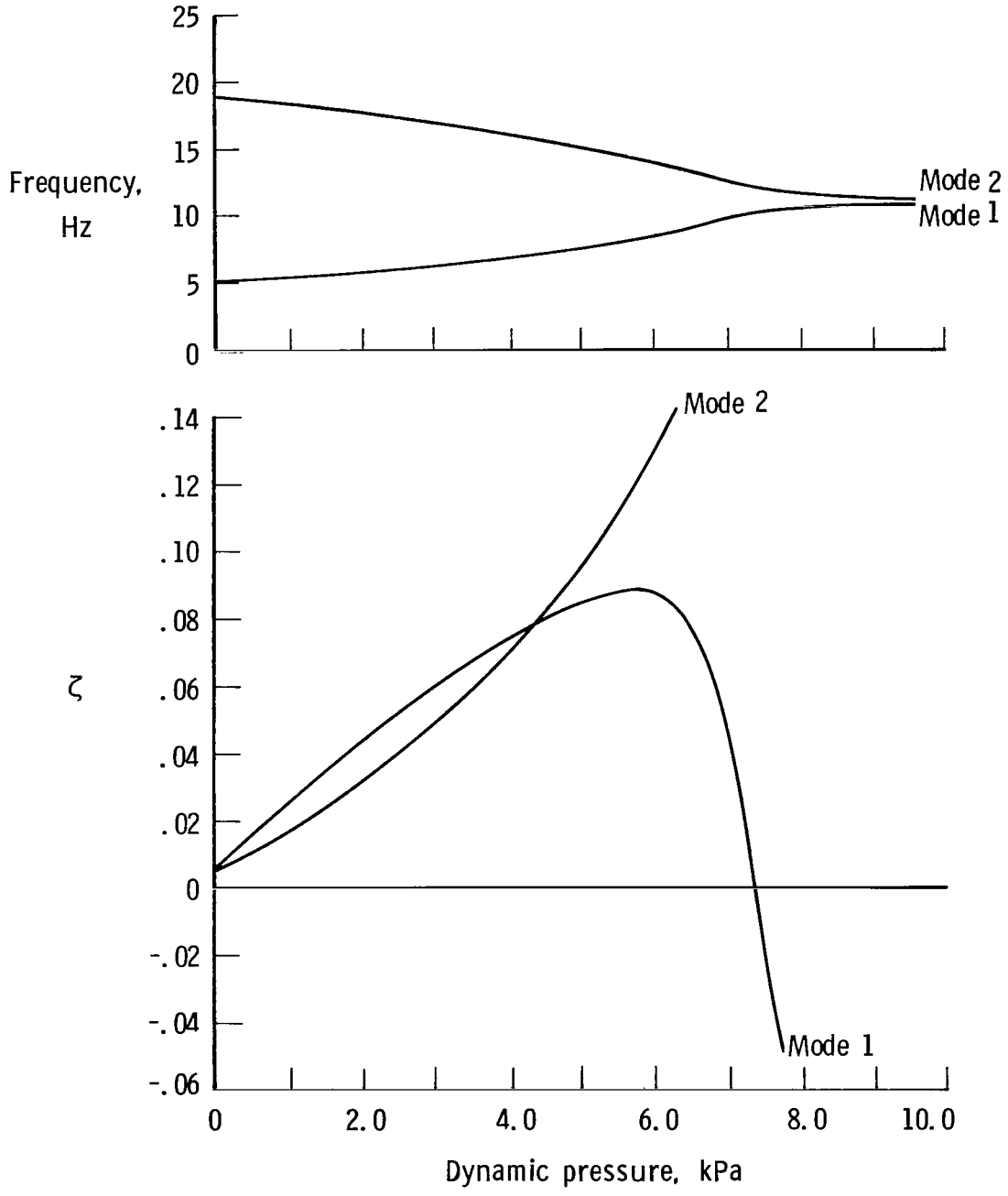

(b) M = 0.60.

Figure 8.- Concluded.

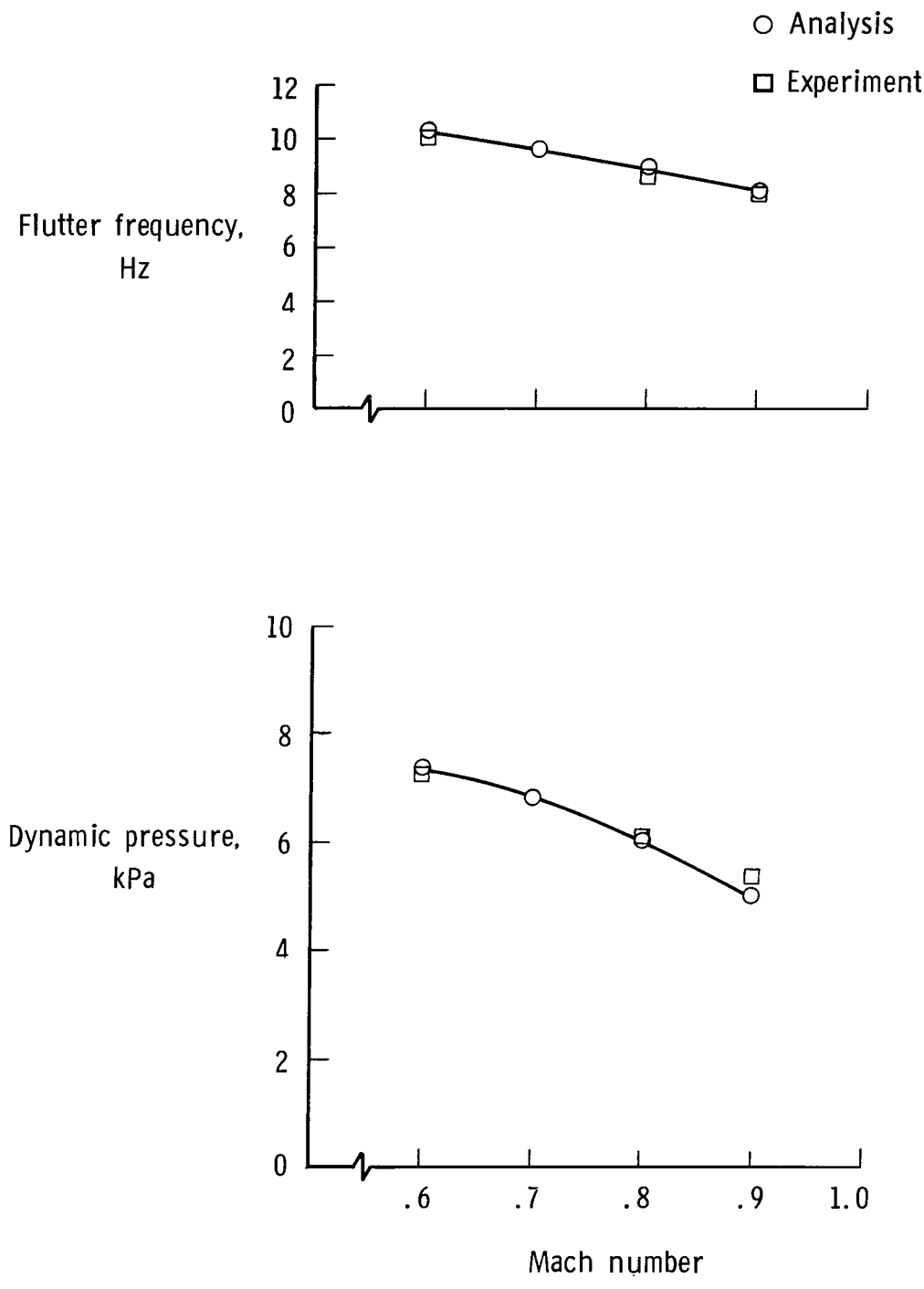

Figure 9.- Comparison of predicted and measured flutter characteristics (system off).

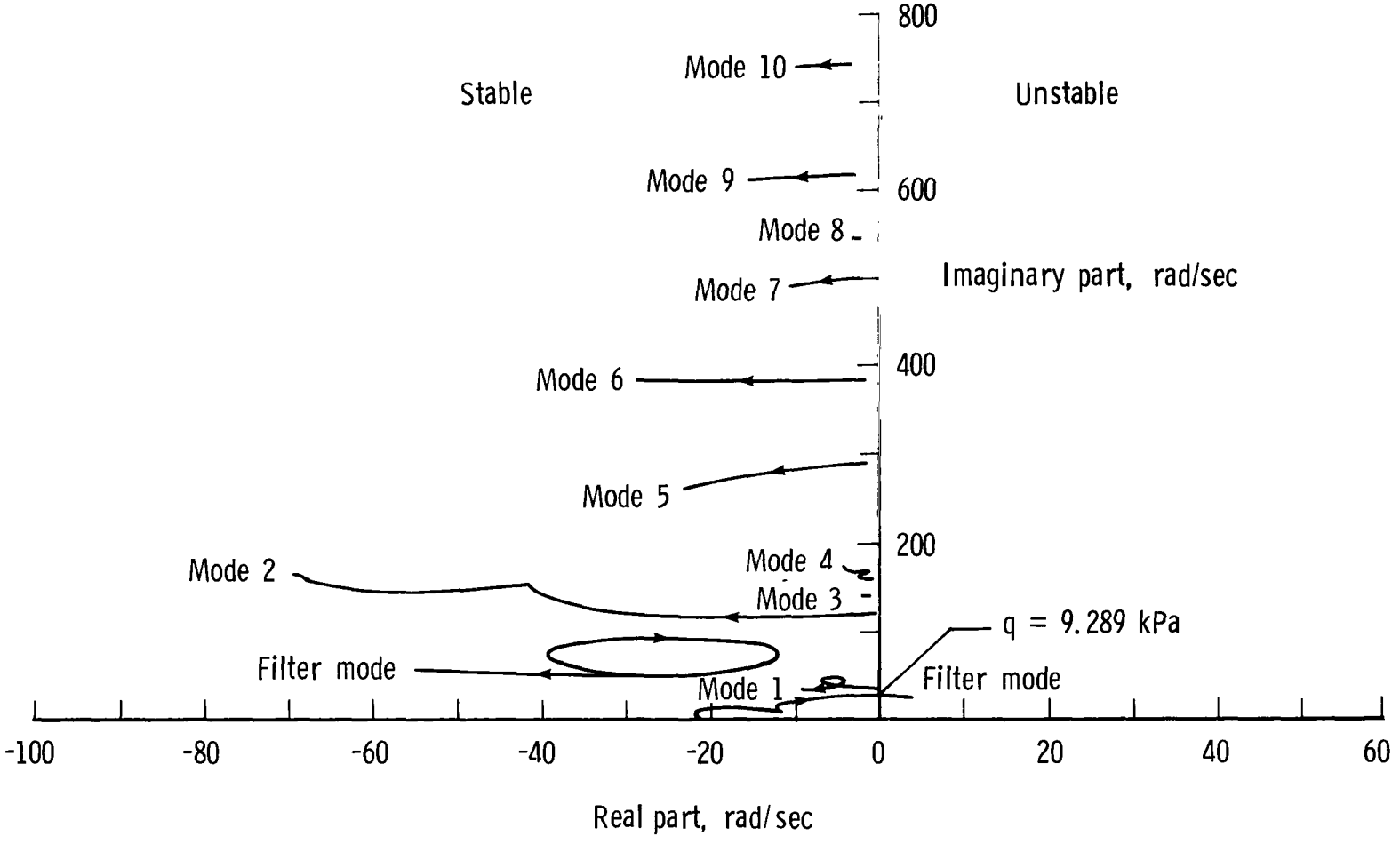

Figure 10.- Dynamic-pressure root locus at M = 0.90 (system on).
Arrows indicate increasing dynamic pressure.

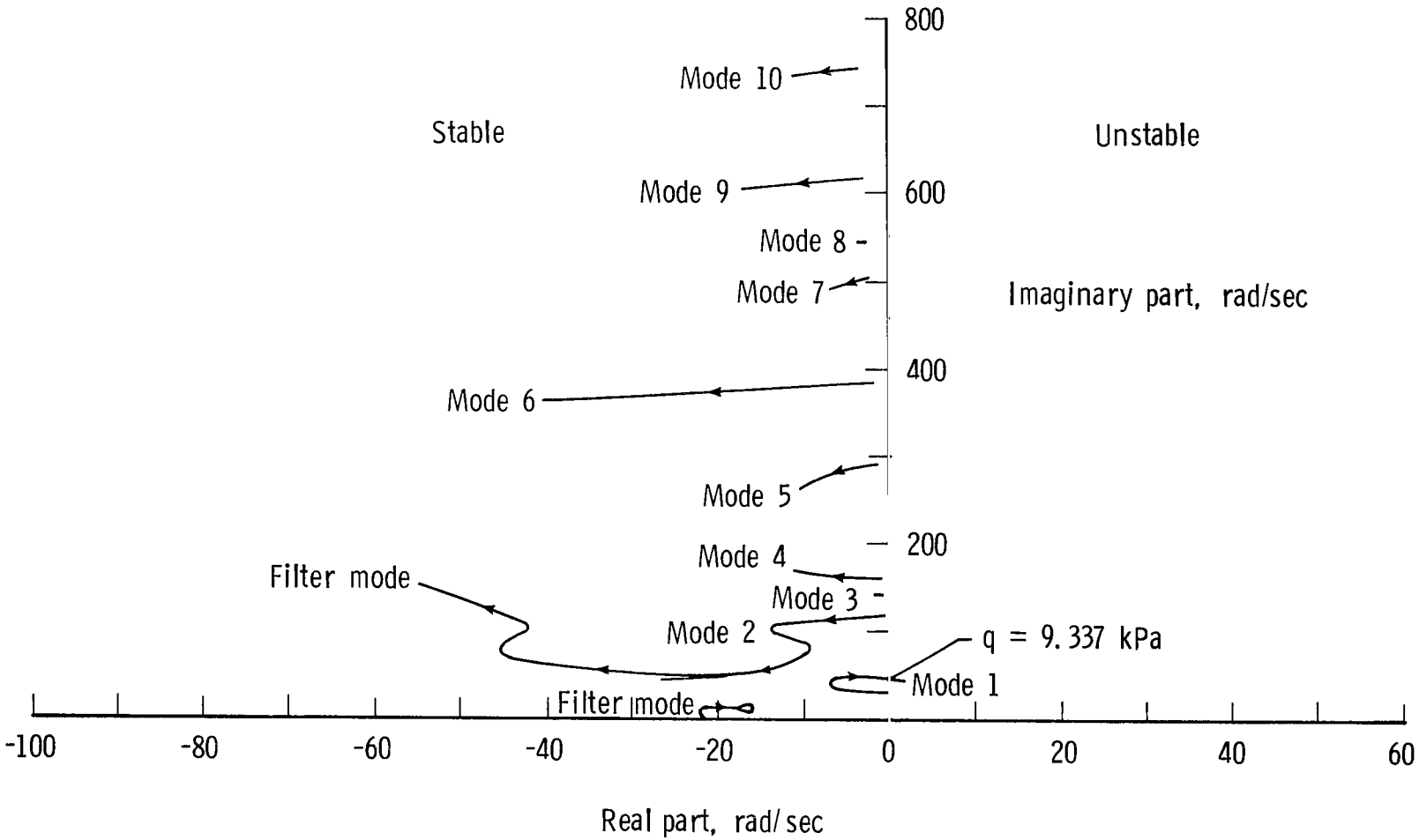

Figure 11.- Dynamic-pressure root locus at M = 0.60 (system on). Arrows indicate increasing dynamic pressure.

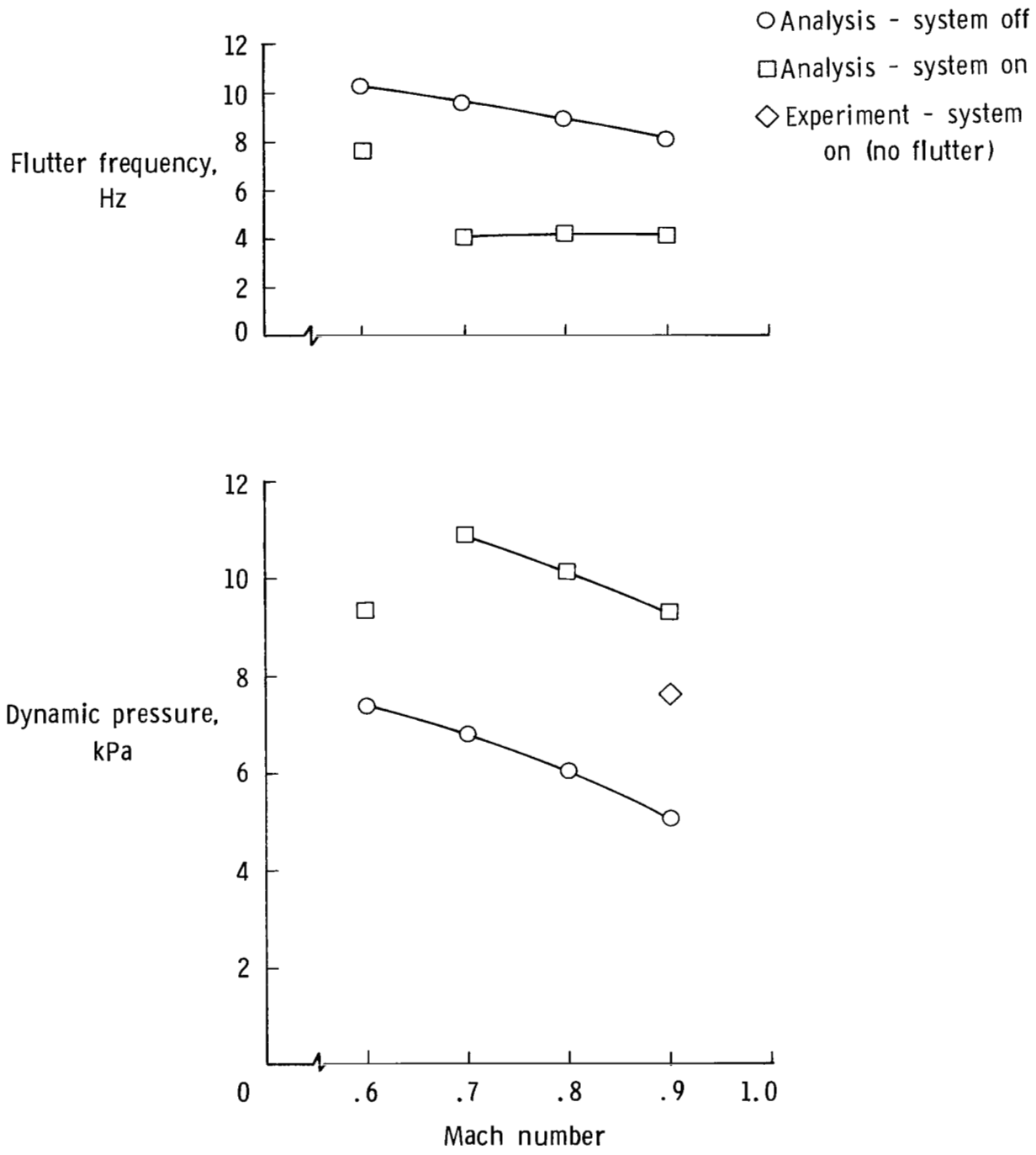

Figure 12.- Effect of control law on flutter dynamic pressure as a function of Mach number.

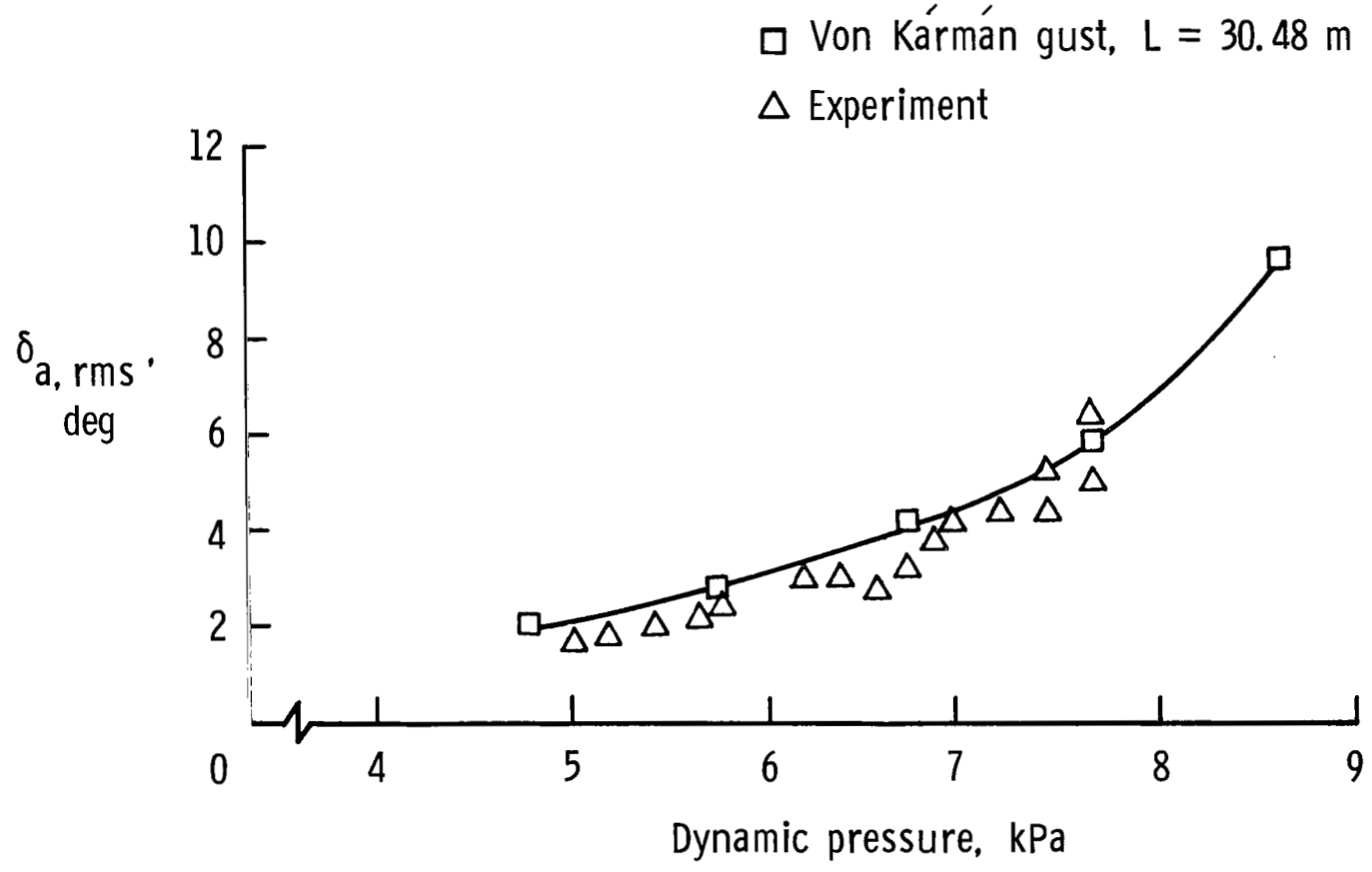

Figure 13.- Variation with dynamic pressure of rms response of control surface at M = 0.90.

1. Report No.	2. Government Accession No.	3. Recipient's Catalog No.
NASA TP-1367		

4. Title and Subtitle	5. Report Date
AN ANALYTICAL TECHNIQUE FOR PREDICTING THE CHARACTERISTICS OF A FLEXIBLE WING EQUIPPED WITH AN ACTIVE FLUTTER-SUPPRESSION SYSTEM AND COMPARISON WITH WIND-TUNNEL DATA	February 1979
	6. Performing Organization Code
7. Author(s)	8. Performing Organization Report No.
Irving Abel	L-12567
9. Performing Organization Name and Address	10. Work Unit No.
NASA Langley Research Center Hampton, VA 23665	505-02-23-02
	11. Contract or Grant No.
12. Sponsoring Agency Name and Address	13. Type of Report and Period Covered
National Aeronautics and Space Administration Washington, DC 20546	Technical Paper
	14. Sponsoring Agency Code

15. Supplementary Notes

16. Abstract

An analytical technique for predicting the performance of an active flutter-suppression system is presented. This technqiue is based on the use of an interpolating function to approximate the unsteady aerodynamics. The resulting equations are formulated in terms of linear, ordinary differential equations with constant coefficients. This technique is then applied to an aeroelastic model wing equipped with an active flutter-suppression system. Comparisons between wind-tunnel data and analysis are presented for the wing both with and without active flutter suppression. Results indicate that the wing flutter characteristics without flutter suppression can be predicted very well but that a more adequate model of wind-tunnel turbulence is required when the active flutter-suppression system is used.

17. Key Words (Suggested by Author(s))	18. Distribution Statement
Flutter suppression Aeroelasticity Analysis	Unclassified - Unlimited Subject Category 39

19. Security Classif. (of this report)	20. Security Classif. (of this page)	21. No. of Pages	22. Price*
Unclassified	Unclassified	42	$4.50

* For sale by the National Technical Information Service, Springfield, Virginia 22161

NASA-Langley, 1979

2 1 1U,D, 012779 S00903DS
DEPT OF THE AIR FORCE
AF WEAPONS LABORATORY
ATTN: TECHNICAL LIBRARY (SUL)
KIRTLAND AFB NM 87117